REMOTE SENS. ENVIRON. 47:345–361 (1994)

Emissivity of Terrestrial Materials in the 3–5 μm Atmospheric Window

*John W. Salisbury** *and Dana M. D'Aria**

Accurate satellite remote sensing of surface temperature has become more and more important in the context of calculating the radiation balance input to climate models for assessment of global change. Surface temperatures can be determined from radiance measurements in both the 3–5 μm and 8–14 μm atmospheric windows, given some estimate of surface emissivity. The 3–5 μm region offers a potential advantage in the accuracy of temperature determination, because temperature estimates are more than two times less sensitive to emissivity errors in this region. However, very little is known about the emissivities of land surface materials in the 3–5 μm region, If emissivities were more variable in the 3–5 μm region than in the 8–14 μm region, this might cancel the advantage of lower sensitivity to emissivity error in the shorter wavelength region. This article documents the directional hemispherical spectral reflectance, from which emissivity can be calculated, of a wide variety of earth surface materials in the 3–5 μm region, and compares their average reflectances in AVHRR Band 3 (3.55–3.93 μm) to that in Bands 4 (10.3–11.3 μm) and 5 (11.5–12.5 μm). It appears from these data that, based on natural variations in emissivity of different surface materials, AVHRR Band 5 is best used for temperature remote sensing of rocks, soils, and senescent vegetation, while Band 3 is best for green vegetation and water. Band 4 is preferred for thermal remote sensing of ice, especially rough ice. Emissivity and reflectivity in the 3–5 μm region affect other significant remote sensing measurements of global change besides those of surface temperature alone. The accuracy of atmospheric sounding of CO near 4.7 μm, for example, depends in part on knowledge of such surface properties to account for surface upwelling radiation. Because of the multiple uses to which our data can be put, digital records of all spectra used in the figures are available from 2.01 μm to 14 μm upon request.

INTRODUCTION

In a previous article (Salisbury and D'Aria, 1992a), we discussed the 8–14 μm emissivity of earth surface materials in the context of the problem of separating temperature and emissivity, which was the theme of the special issue of *Remote Sensing of Environment* in which it was published. Indeed, accurate satellite remote sensing of surface temperature has become more and more important in the context of calculating radiation balance input to climate models for assessment of global change. While remote sensing of sea surface temperature has been rather successful (McClain et al., 1985) due to the relative uniformity of the target, the variability of land surface materials and general ignorance of their emissivities has made land remote sensing more difficult (Price, 1983). Simplifying assumptions are often used over a variable surface, such as that all polar ice is snow-covered (Key and Haefliger, 1992), or that land surfaces simply emit as black bodies (Price, 1983). Clearly, more detailed knowledge of surface emissivities is necessary for more accurate temperature measurements, and our previous article began the task by documenting emissivity of surface materials in the 8–14 μm region.

While the 8–14 μm atmospheric window is widely used in remote sensing of temperature, because typical earth surface temperatures produce peak radiance in that wavelength range, the 3–5 μm window may also be useful. Volcanic eruptions and fires exhibit peak radiance in the shorter wavelength region, but this region has a significant potential advantage for remote sensing of cooler temperatures as well. This advantage is revealed by a Planck's law calculation showing that the temperature error in the shorter wavelength region

*Department of Earth and Planetary Sciences, Johns Hopkins University, Baltimore

Address correspondence to John Salisbury, Dept. of Earth and Planetary Sciences, Johns Hopkins University, 34th and Charles Streets, Baltimore, MD 21218.

Received 6 November 1992; revised 3 April 1993.

0034-4257/94/$7.00

655 Avenue of the Americas, New York, NY 10010

due to an error in estimating emissivity is less by a factor of more than 2 (that is, at average Earth temperatures an emissivity error of 0.01 results in a temperature error of approximately 0.25°C at 4 μm, compared to a temperature error or 0.6°C at 10 μm). Since surface temperature accuracy is so important in radiation balance calculations, this reduced sensitivity to emissivity error advantage of the 3–5 μm region might easily outweigh the energy disadvantage. However, the range of temperature error in each wavelength region depends on the range of emissivities found there. The emissivity range for the 3–5 μm region has been very poorly known (Hovis and Callahan, 1966), and it is the purpose of this article to correct this deficiency by documenting the 3–5 μm emissivities of a wide variety of earth surface materials. We tabulate the average emissivity of these materials in Advanced Very High Resolution Radiometer (AVHRR) Band 3 (3.55–3.93 μm) and, for convenient comparison, in Bands 4 (10.3–11.3 μm) and Band 5 (11.5–12.5 μm) as well.

This tabulation of reflectances in AVHRR band regions illustrates one application of these spectral data. However, emissivity and reflectivity in the 3–5 μm region affect many other significant remote sensing measurements of global change besides those of surface temperature alone. The accuracy of atmospheric sounding of CO near 4.7 μm, for example, depends in part on knowledge of such surface properties to account for surface upwelling radiation. Thus, several instruments on board the Earth Observing System (EOS) will need emittance and reflectance data in the 3–5 μm and 8–14 μm atmospheric windows (e.g., Fujisade and Ono, 1991; Salomonson et al., 1989; Drummond, 1991). Because of the multiple uses to which our data can be put, digital records of all spectra used in the figures are available from 2.01 μm to 14 μm upon request (see below).

EXPERIMENTAL TECHNIQUE

The details of sample acquisition and measurement technique are given in Salisbury and D'Aria (1992a). Briefly, near-normal (10°) directional hemispherical reflectance spectra of well-characterized samples were measured on a Nicolet System 510 FTIR spectrometer with 4 wavenumber resolution throughout the spectral range from 2.08 μm to 14 μm. These reflectance spectra can be used to predict directional emissivity using Kirchhoff's law, as demonstrated with emittance spectra of quartz sand (Salisbury and D'Aria, 1992a). For igneous rocks, most spectra are of freshly broken rock surfaces. For sedimentary and metamorphic rocks, very coarsely particulate (250–1500 μm size range) material was used as a good analog of a fresh, rough surface.

Digital data are recorded for each spectrum. The data used in the figures illustrating the spectral behavior of different types of surface materials can be obtained from the senior author by sending him three high density 3.5 in. disks, and specifying MS-DOS or Macintosh format for the digital data.

SPECTRAL BEHAVIOR OF ROCKS

Igneous Rocks

Spectra of suites of igneous rocks have been published by several other authors (e.g., Lyon, 1964), but, with the exception of spectra of two igneous rocks by Hovis and Callahan (1966), all others have skipped the 3–5 μm region, except for Salisbury et al. (1988). Figure 1 shows representative spectra taken from Salisbury et al. (1988) of the full range of igneous rock types from felsic to ultramafic. With the exception of quartz, the spectra of major igneous rock-forming minerals are featureless in the 3–5 μm region. They usually display a broad reflectance maximum in the middle of the region because of absorption bands at shorter wavelengths due to water in fluid inclusions, and at longer wavelengths due to overtone / combination tone bands of the fundamental molecular vibration bands in the 8–20 μm region [the origins of molecular vibration bands in minerals are discussed in detail in Farmer (1974), Farmer and Palmieri (1975), and Estep-Barnes (1977) and summarized in Salisbury et al. (1992)]. By contrast, the basalt spectrum (dash–dot curve in Fig. 1) shows a lack of fluid inclusions in the minerals comprising the basalt by the rise in reflectance toward 3 μm. The granite spectrum shows the presence of quartz by the very weak quartz absorption bands near 4.5 μm and 4.7 μm,

Figure 1. Directional hemispherical reflectance spectra of rough surfaces of igneous rocks, including a basalt (dash–dot curve), granite (dotted curve), syenite (solid curve), and dunite (dashed curve).

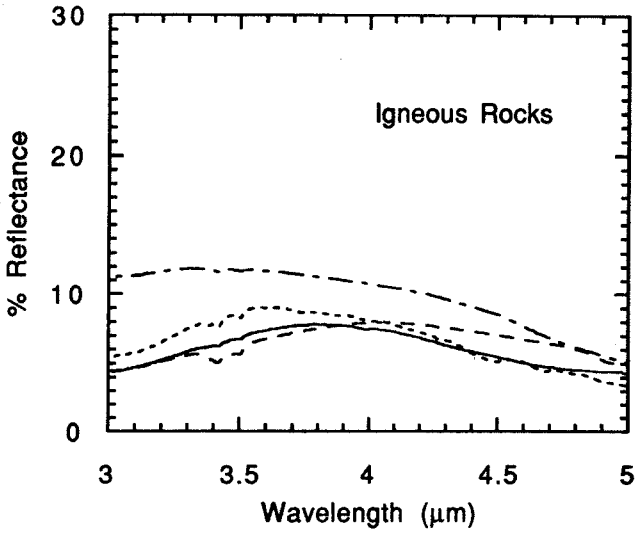

Table 1. Average Reflectances from 3.55–3.93 μm (AVHRR Band 3), 10.3–11.3 μm (AVHRR Band 4), and 11.5–12.5 μm (AVHRR Band 5)

Samples	*Filename*	*% Reflectance*		
		Band 3	*Band 4*	*Band 5*
Rocks				
Igneous	Aplite.h1	16.74	8.37	4.41
	Granite.h1	8.72	8.54	4.80
	Granite.h2	12.54	8.88	4.62
	Granite.h3	9.45	7.07	3.53
	Granite.h5	9.16	7.04	3.56
	Obsidian.h1	4.83	11.31	5.48
	Rhyolite.h1	16.42	9.58	4.82
	Andesite.h1	4.24	10.41	5.22
	Andesite.h2	11.87	6.68	3.46
	Andesite.h4	6.95	9.59	4.18
	Diorite.h1	12.81	9.09	4.49
	Granodior.h1	10.63	10.60	5.47
	Granodior.h2	4.71	9.54	4.71
	Monzonite.h1	12.45	8.95	4.80
	Qmonzonite.h1	11.67	7.00	3.30
	Syenite.h1	7.60	10.06	5.08
	Syenite.h2	14.26	8.80	4.18
	Tonalite.h1	12.19	11.26	5.58
	Anorthosite.h1	8.54	7.40	3.97
	Basalt.h1	3.57	9.57	5.00
	Basalt.h2b	7.05	10.44	6.81
	Basalt.h5	11.11	13.36	7.15
	Basalt.h7	11.40	9.66	4.74
	Basalt.h9	9.24	11.08	5.42
	Basalt.h10	13.39	11.91	6.41
	Diabase.h1	9.84	11.02	6.09
	Diabase.h2	8.55	11.59	6.16
	Gabbro.h1	7.41	12.87	5.64
	Ijolite.h1	14.92	8.84	5.26
	Lamprophyre.h1	5.39	10.84	6.06
	Norite.h1	14.29	10.10	4.48
	Norite.h2	4.99	12.36	6.33
	Dunite.h1	7.24	14.60	5.23
	Picrite.h1	11.31	28.81	12.24
	Picrite.h2	16.13	14.79	6.65
Sedimentary	Greywacke.h1	15.94	5.01	2.77
	Limestone.h1	10.58	5.57	3.40
	Limestone.h2	10.58	6.37	3.40
	Limestone.h3	4.72	9.43	3.49
	Sandstone.h1	16.81	3.60	2.20
	Sandstone.h2	11.52	3.23	2.07
	Sandstone.h3	12.17	4.02	2.54
	Sandstone.h4	13.65	4.02	2.54
	Sandstone.h5	36.18	4.21	2.69
	Shale.h1	13.61	2.61	1.86
	Shale.h2	6.03	3.55	2.50
	Shale.h3	11.05	3.53	2.86
	Shale.h4	5.28	2.99	2.31
	Shale.h5	8.79	3.15	2.15
	Shale.h6	5.21	3.34	2.68
	Siltstone.h1	23.82	3.69	2.96
	Siltstone.h2	28.93	3.25	2.22
Metamorphic	Gneiss.h1a	31.99	4.03	2.56
	Gneiss.h3	26.12	5.07	2.77
	Gneiss.h4	18.08	6.46	3.29
	Hornfels.h1a	19.50	6.08	3.41
	Marble.h2	5.47	4.67	2.37
	Marble.h3	9.77	5.09	4.62
	Marble.h4	8.85	6.51	4.74

Table 1. (continued)

Samples	*Filename*	*% Reflectance*		
		Band 3	*Band 4*	*Band 5*
	Marble.h5	7.70	4.77	2.92
	Phyllite.h1	7.04	7.63	4.93
	Quartzite.h1	22.04	2.81	1.97
	Quartzite.h4a	28.30	4.74	2.98
	Quartzite.h6	32.51	4.63	2.90
	Schist.h3a	10.24	5.80	3.80
	Schist.h6a	45.06	10.34	4.36
	Schist.h7	22.04	8.59	4.15
	Slate.h1a	11.38	5.30	3.05
	Slate.h2a	18.91	5.19	3.02
	Slate.h3	4.11	4.18	2.73
Rock Coatings				
Desert varnish	Rhyolite.f[a]	19.67	5.21	3.06
	Rhyolite.v[b]	11.26	8.65	4.53
	Basalt.f[a]	5.88	8.65	4.53
	Basalt.v[b]	7.42	4.67	3.34
	Ijolite.f[a]	7.42	4.67	3.34
	Ijolite.v[b]	12.66	7.05	4.83
Lichens	Crustose.10	8.60	4.02	2.66
	Crustose.65	10.39	4.11	3.35
Soils				
Entisols	0135	17.12	3.55	2.18
	0149	8.75	2.40	1.89
	2230	14.31	2.70	1.95
Vertisols	0475	13.64	2.69	1.99
Inceptisols	0138	10.43	2.41	1.91
	0215	10.36	2.84	1.95
	0224	10.25	3.48	2.73
	0226	16.71	3.13	2.34
	0227	11.65	3.68	2.42
	0209	25.34	3.61	3.05
	2671	14.58	2.29	2.11
Aridisols	0139	27.82	3.20	2.76
	0147	28.41	4.77	2.68
	0148	33.14	3.28	3.48
	0150	9.95	2.12	1.63
	0151	28.40	3.01	2.76
	0152	23.29	2.29	2.36
	2659	22.89	2.65	2.85
	1530	21.74	3.21	2.88
	1536	22.95	2.85	2.61
	3721	21.50	2.36	2.37
	2695	25.48	2.82	3.05
Mollisols	0134	20.75	3.12	2.24
	0140	24.53	2.93	2.35
	0211	16.24	2.68	2.05
	0212	11.62	2.57	2.09
	0213	20.40	2.50	2.27
	0216	19.20	2.22	1.86
	0225	12.46	2.77	2.07
Spodosols	0127	10.99	3.04	2.86
Alfisols	0128	29.60	3.44	2.77
	0129	20.13	3.57	2.34
	0132	22.62	3.10	2.31
	0133	26.02	3.02	1.98
	0137	20.60	3.34	2.29
	0214	19.46	2.62	2.28
	0217	11.90	2.71	2.48
	0219	22.89	3.55	2.42
	0221	22.06	2.99	1.91
	0222	27.23	3.46	2.66

Table 1. (continued)

Samples	*Filename*	*% Reflectance*		
		Band 3	*Band 4*	*Band 5*
Ultisols	0136	22.24	3.86	2.42
	0145	27.65	4.70	2.81
	0146	32.52	4.89	3.16
	0208	24.13	4.22	3.16
	0210	27.39	4.03	3.12
	0223	29.76	4.63	2.99
	0220	21.08	4.00	2.67
Oxisols	4717	11.08	1.73	1.35
Vegetation				
Lichens	Foliose.1	6.36	3.13	2.02
	Foliose.2	5.77	2.90	2.08
	Fruticose.1	4.93	2.89	2.18
Green foliage	Beech (*Fagus grandifolia*)	4.91	4.72	3.99
	Cherry (*Prunus serotina*)	3.17	3.55	2.89
	Hickory (*Carya glabra*)	4.85	1.82	1.61
	Laurel (*Kalmia latifolia*)	4.13	4.68	4.64
	Redmaple (*Acer rubrum*)	3.64	4.70	3.82
	Redoak (*Quercus rubra*)	3.38	5.29	5.35
	Sugarmaple (*Acer saccgaryn*)	3.20	4.41	3.45
	Yellowpoplar (*Liriodendron tuliperfera*)	3.51	3.23	2.17
	Conifer (*Pinus sp.*)	2.32	2.04	2.03
	Cedar (*Cedrus deodara*)	2.20	2.17	2.23
	Whitepine (*Pinus strobus*)	2.38	2.21	1.83
	Bigbluestem (*Andropogon gerardii*)	3.23	3.58	2.22
	Indiangrass (*Serghastrum nutans*)	3.19	3.77	2.35
	Switchgrass (*Panicum virgatum*)	4.64	3.35	2.75
	Moss (unknown)	4.32	1.99	1.65
Senescent foliage	Senbeech (*Fagus grandifolia*)	24.83	17.67	14.84
	Senredoak.h1 (*Quercus rubra*)	15.53	9.26	8.25
	Senpine (*Pinus strobus*)	3.86	2.25	1.94
	Senryegrass (*Secale cereale*)	15.12	8.94	8.61
Tree bark	Beechbark (*Fagus grandifolia*)	11.75	4.16	4.59
	Oakbark.1 (*Quercus alba*)	12.23	8.10	8.93
	Oakbark.2 (*Quercus rubra*)	8.78	4.42	4.71
	Ypoplarbark (*Liriodendron tuliperfera*)	12.57	6.29	5.84
	Pinebark.1 (*Pinus taeda*)	9.04	5.13	5.23
	Grapebark (*Vitus sp.*)	6.99	4.13	3.67
Decomposing soil litter	Wood	8.85	3.48	3.23
	Deciduous	7.63	3.99	3.67
	Coniferous	6.42	2.40	1.84
Water and ice				
Water	Seawater	2.53	0.961	1.40
	Distwater	2.51	0.93	1.45
Ice	Seaice.smooth	3.85	2.31	2.72
	Seaice.100grit	7.45	1.44	2.94
	Distice.smooth	3.04	2.36	6.38
	Distince.100grit	5.35	1.35	2.83
Suspended sediment	Qtzwater.7	2.53	1.16	1.58
	Qtzwater.23	2.54	1.07	1.55
	Qtzwater.64	2.54	0.973	1.54
Water coatings	Foam	3.36	0.955	1.31
	Oil15465	3.95	3.77	3.77
	Oil35473	3.77	3.63	3.63
	Oil34792	4.15	4.03	4.01
	Oil39076	4.28	4.43	4.47
	Oil42667	4.17	3.67	3.60
	Qtzfloat	2.61	1.68	1.72
	Soilfloat	2.67	1.71	1.81

[a] Fresh surface.
[b] Varnish.

which are better displayed in spectra of quartz-rich sedimentary and metamorphic rocks discussed below.

Table 1 shows the reflectances of different Earth surface materials convolved with AVHRR Bands 3, 4, and 5, assuming square filters in these bands. Igneous rock spectra display their greatest variation in reflectance in AVHRR Bands 3 and 4, but for different reasons in the different bands. The variability of reflectance in Band 3, and the lack of dependence of this variability on rock type, are due to the relative transparency of all silicate rock-forming minerals in this region (Salisbury et al., 1992). Photons enter such semitransparent minerals easily, and the number backscattered depends on the roughness of the surface and the abundance of scattering centers (grain boundaries, cracks, fluid and solid inclusions, etc.) below the surface. Because the surface roughness and abundance of scattering centers is highly variable from rock to rock, the reflectance is also.

Band 4, on the other hand, lies in a wavelength region that commonly includes the fundamental molecular vibration ("reststrahlen") bands. The wavelength of these features varies systematically with mineralogy, which has been known for quite a long time (Lyon, 1964), and which was illustrated in Salisbury and D'Aria (1992a). The intensity of these reststrahlen bands does vary with surface roughness, but most of the samples measured have comparably rough, freshly broken surfaces. Thus, the reflectance variations in Band 4 (Table 1) are primarily a function of composition.

Band 5 (Table 1) shows relatively little variation in reflectance for igneous rocks compared to Bands 3 and 4, because it lies to longer wavelength than the most intense reststrahlen bands (with the exception of one of the picrites).

Sedimentary Rocks

Very few spectra of sedimentary rocks covering the 3–5 μm region are available in the open literature. In fact, we could find only one such spectrum (Hovis and Callahan, 1966), as both Hunt and Salisbury (1975) and Lang et al. (1990) skipped this wavelength region. Consequently, we show a relatively large number of representative spectra in Figure 2, and comment briefly on their individual spectral features. Generally speaking, it is apparent from the relatively low reflectance and lack of variability in Band 4 of Table 1 that sedimentary rocks do not display strong reststrahlen bands in Band 4, in contrast with igneous rocks. This is because silicate minerals having reststrahlen bands in this region, such as feldspars and mafic minerals, are relatively scarce in sedimentary rocks. At the same time, the carbonate minerals common in sedimentary rocks typically display their bending vibration bands between Bands 4 and 5. On the other hand, carbonate minerals usually display strong absorption bands in the 3–5 μm region. This increases the reflectance variations in Band 3, as the effects of compositional differences add to the effects of differences in surface roughness and the abundance of scattering centers.

The spectra of sandstones (Fig. 2a) are typically dominated by the reflectance of quartz, as illustrated by the dotted curve. This shows a peak reflectance near 3.92 μm, with a falloff toward shorter wavelength due to absorption by water in fluid inclusions near 2.9 μm, and toward longer wavelength due to the increasing strength of Si—O overtone / combination tone bands near 4.29 μm, 4.48 μm, 4.69 μm, and 4.95 μm.

Many quartz grains in sandstone are cemented by carbonate, which displays strong absorption bands that affect AVHRR Band 3. The ferruginous sandstone (solid curve in Fig. 2a) has such a cement, and the two doublets near 3.36 / 3.49 μm and 3.85 / 3.99 μm are the resulting carbonate bands.

In Figure 2b the graywacke spectrum (solid line) displays weak quartz overtone / combination bands, but otherwise shows the typical broad rise in reflectance centered near 4 μm, as does the feldspatic siltstone spectrum. The argillaceous siltstone (dashed curve) also contains carbonate, as demonstrated by the presence of the stronger carbonate doublet near 3.85 / 3.99 μm. These materials have a generally higher reflectance than sandstones because of their smaller grain size (4–63 μm, as compared to 63 μm–2 mm), which increases backscatter.

Figure 2c illustrates spectra of typical shales. The calcareous shale spectrum (dotted curve) displays very strong carbonate bands, including features near 4.3 μm and 4.7 μm that overlap with quartz absorption bands. These features are so weak that they are not usually seen unless carbonate is very abundant or the bands are enhanced by the scattering induced by very fine particle size. The carbonaceous shale spectrum (dashed curve) has a low reflectance due to the presence of opaque organic matter, but weak carbonate bands can still be discerned. The illitic shale contains a little carbonate, but the spectrum (solid curve) has the largely featureless broad rise associated with all silicates lacking spectral features in this region.

Not surprisingly, the limestone spectra in Figure 2d display very strong carbonate bands. As in the case of the carbonaceous shale, however, the carbonaceous limestone spectrum (dotted curve) has a low reflectance due to the high opacity of the disseminated organic matter. Major spectral features for the dolomitic limestone (dashed curve) are shifted to shorter wavelength than those exhibited by the calcareous limestone (solid curve), due to the substitution of Mg for Ca, and additional bands occur near 4.29 μm and 4.43 μm. Note that the weak spectral features in the carbonaceous limestone, partially masked by the opaque carbonaceous

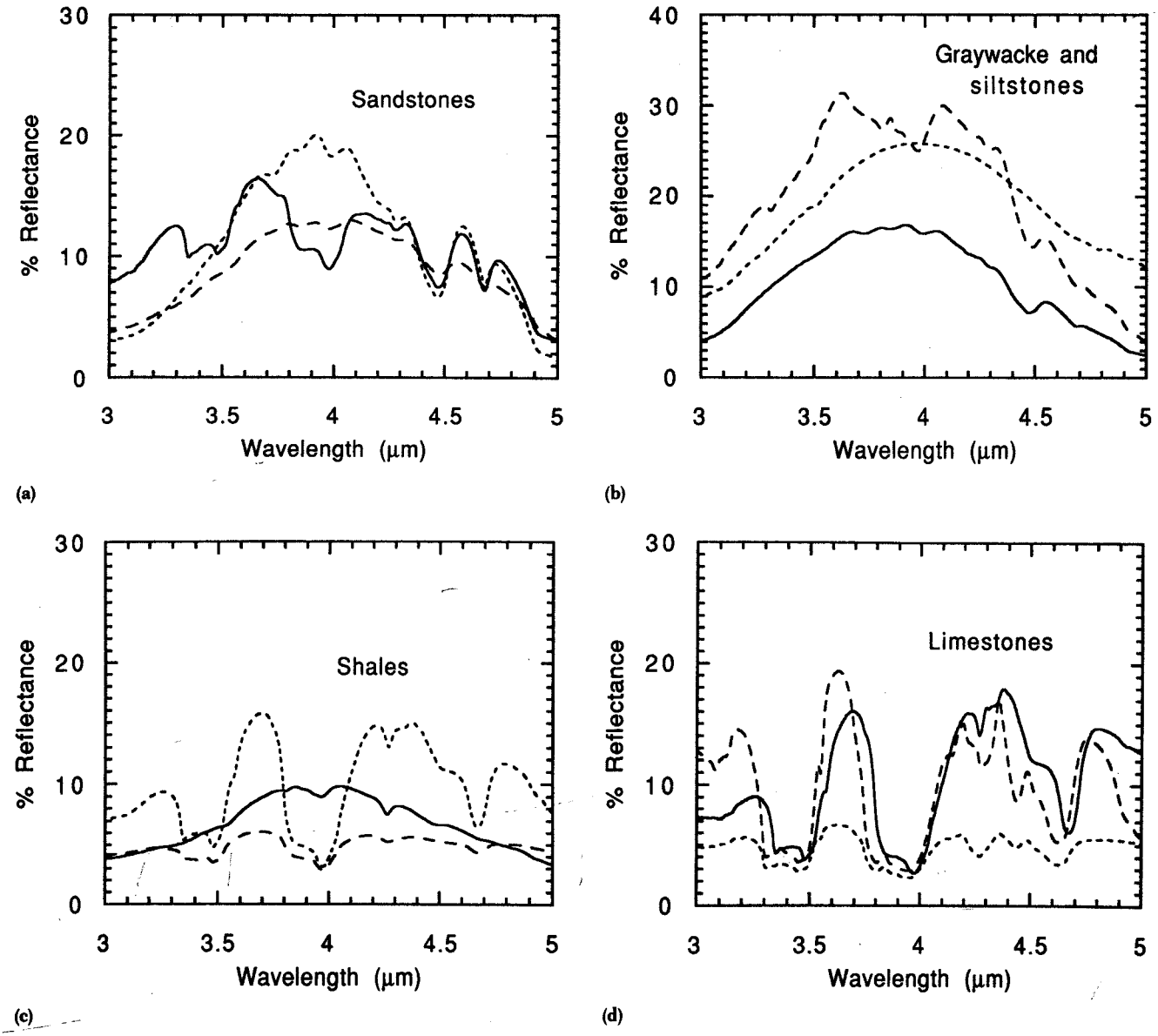

Figure 2. Directional hemispherical reflectance spectra of coarsely particulate (250–1500 μm size range) samples of different sedimentary rocks: a) sandstones, including ferruginous (solid curve), glauconitic (dashed curve), and arkosic (dotted curve) samples; b) graywacke (solid curve) and argillaceous (dashed curve) and feldspathic (dotted curve) siltstones; c) shales, including illitic (solid curve), carbonaceous (dashed curve), and calcareous (dotted curve); d) limestones, including fossiliferous (solid curve), dolomitic (dashed curve), and carbonaceous (dotted curve) samples.

material, clearly indicate by their wavelength positions that the carbonate present is dolomitic.

Metamorphic Rocks

As in the case of sedimentary rocks, we were unable to find more than a single spectrum of a metamorphic rock covering the 3–5 μm region (Hovis and Callahan, 1966), because Hunt and Salisbury (1976) skipped this wavelength region. Thus, we also present a relatively large number of metamorphic rock spectra in Figure 3 and briefly discuss the spectral features of individual samples. Generally speaking, metamorphic rock spectra display slightly more variability in AVHRR Bands 4 and 5 than do sedimentary rocks because of the greater variability in their compositions. However, it is Band 3 that shows the greatest variability, exceeding that of both sedimentary and igneous rocks, because of the more strongly expressed absorption bands of the recrystallized minerals in metamorphic rocks.

Despite the variation in composition of the gneisses for which spectra are shown in Figure 3a, the spectra

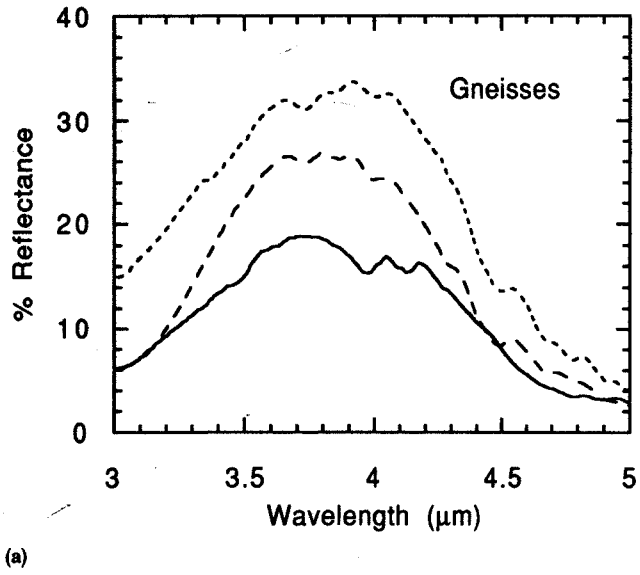

(a)

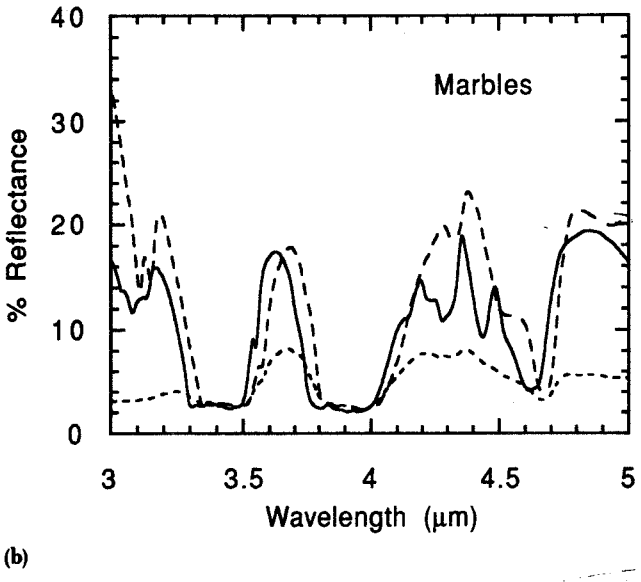

(b)

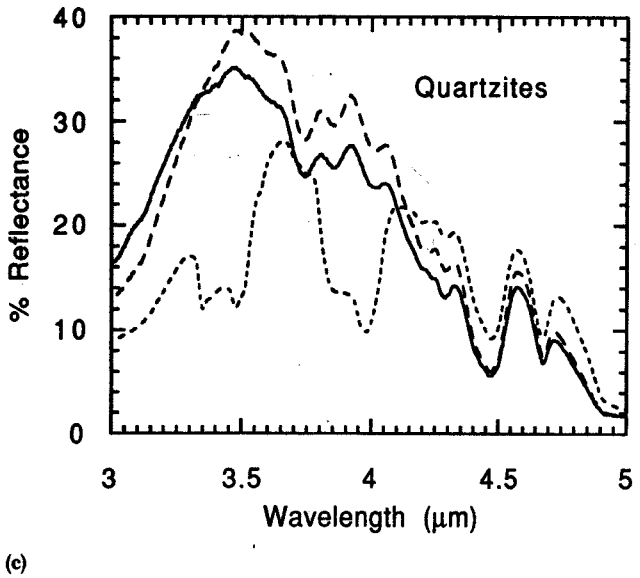

(c)

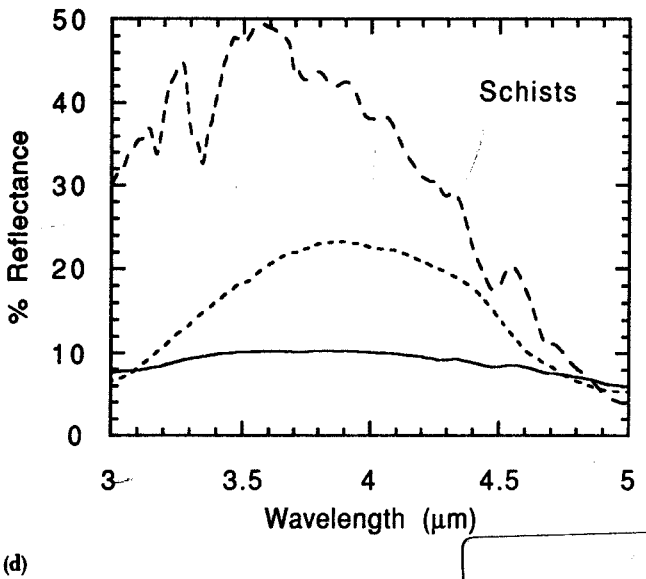

(d)

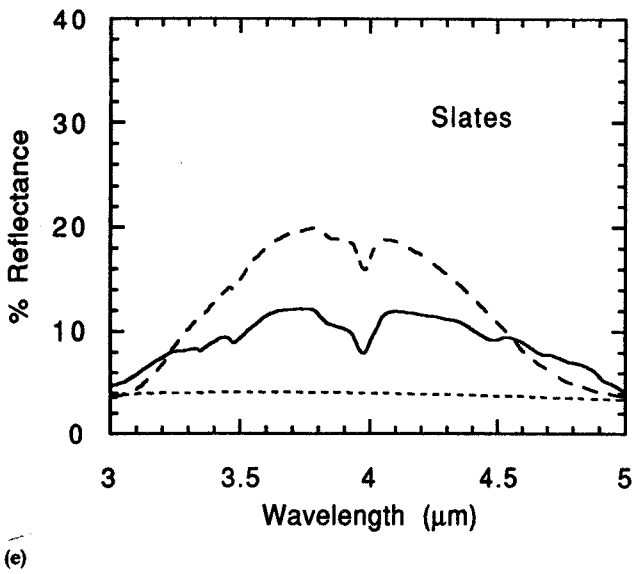

(e)

Figure 3. Directional hemispherical reflectance spectra of coarsely particulate (250–1500 μm size range) samples of different metamorphic rocks: a) gneisses, including syenitic (solid curve), felsitic (dashed curve), and chloritic (dotted curve); b) marbles, including dolomitic (solid curve), calcitic (dashed curve), and serpentinitic (dotted curve); c) quartzites, including purple (solid curve), green (dashed curve), and red (dotted curve); d) schists, including muscovite schist (solid curve), tremolite schist (dashed curve), and chlorite schist (dotted curve); e) slates, including gray slate (solid curve), green slate (dashed curve), and chiastolic slate (dotted curve).

themselves show little variation from the overall broad silicate rise in reflectance in the middle of the 3–5 μm range. Both the felsitic (dashed curve) and chloritic (dotted curve) gneiss spectra also display very weak quartz overtone / combination bands, while the syenite gneiss spectrum (solid curve) has a weak 3.97 / 4.12 μm doublet that we cannot explain.

Figure 3b shows spectra of typical marbles. As in the case of the limestone spectra described above, major spectral features for the dolomitic marble (solid curve) are characteristically shifted slightly to shorter wavelength than those of the calcitic marble (dashed curve) by the substitution of Mg for Ca, and two additional bands occur near 4.29 μm and 4.43 μm. The presence of an opaque mineral (magnetite?) in the serpentinitic marble (dotted curve) greatly reduces reflectance throughout the wavelength region, as well as partially masking the carbonate bands.

Figure 3c shows spectra typical of quartzites. The color of quartzites is usually caused by trace amounts of different ferric oxide minerals or widely disseminated fine mica. Thus, our purple and red quartzites are colored by ferric oxide, while the green sample contains fine chlorite. These colorants have no spectral signatures in the 3–5 μm region, and, consequently, most quartzite spectra are totally dominated by quartz overtone / combination tone bands superimposed on the broad rise in reflectance, as in the case of our purple (solid curve) and green (dashed curve) quartzites. The red quartzite (dotted curve), however, has calcite filling the interstices between quartz grains and displays strong carbonate bands as well.

Spectra of schists are shown in Figure 3d. Most schists derive their schistosity from micas, and thus the spectra of our chlorite (dotted curve) and muscovite schists (solid curve) are more typical than that of the tremolite schist (dashed curve). The latter has a very high reflectance (note scale change) and displays characteristic tremolite overtone / combination tone bands near 3.18 μm and 3.35 μm, plus weak quartz features at longer wavelengths.

Spectra of slates in Figure 3e show a wide range of reflectance due primarily to the very low reflectance of the chiastolic slate (dotted curve) associated with the presence of very abundant opaque organic matter. Spectra of the gray (solid curve) and green (dashed curve) slates show evidence of minor calcite in the weak carbonate bands near 3.5 μm and 4 μm, and the gray slate also displays weak quartz bands near 4.5 μm and 4.7 μm.

The Effect of Rock Coatings on Emissivity

Desert varnish in the United States is typically composed of manganese and ferric oxides intimately mixed with montmorillonitic clay (Potter and Rossman, 1979), but may contain kaolinitic clay in Western Australia (R. Lyon, personal communication). This varnish material commonly coats the surfaces of rocks in a desert environment, and the clay Si—O reststrahlen band may substantially mask the rock spectrum in the 8–14 μm region as the varnish thickens. Rock specimens selected to illustrate this effect in the previous article (Salisbury and D'Aria, 1992a) had continuous coatings of varnish that were sufficiently thick to completely obscure the underlying mineral grains from view, and their spectra were dominated by the clay reststrahlen band near 9.7 μm.

Figure 4 shows the effect of these coatings in the 3–5 μm region. Figure 4a depicts the spectrum of a fresh surface of a rhyolite (solid curve) compared to that of a completely coated surface (dashed curve). The spectrum of the varnish coating is featureless in this region. Its relative opacity reduces the reflectance, especially at the shorter wavelength end of the 3–5 μm region, and effectively masks most of the spectral features in the fresh rhyolite spectrum. These spectral features are due, oddly enough, primarily to a small amount of calcite, instead of to the quartz which is also present.

Figures 4b and 4c illustrate the effect of varnish coatings on mafic and ultramafic rocks, the spectra of which are fairly featureless to begin with. In both cases, the relative opacity of varnish and substrate is reversed compared to the rhyolite. Thus, the varnish coating (dashed curve) slightly raises the reflectance, especially at the long wavelength end of the window. Otherwise, the spectral effect is small.

Vegetation may also mask the spectral signatures of underlying rocks, changing their reflectivities and emissivities. When green trees or shrubs are present in sufficient density, they are easily distinguished in remote sensing data by their characteristic reflectance signature in the visible / near-infrared. The mixing model problem becomes more difficult when the vegetation is very sparse and / or senescent, and senescent grass is a particularly common scene contaminant. However, lichen coatings on rocks may have the most subtle effect on rock emissivity, because they are not obvious, unless outcrops are observed closely in the field. In the 8–14 μm region, lichen acted as almost a neutral mask on the rock spectrum, reducing the height of the reststrahlen reflectance peaks roughly in proportion to area of coverage. Figure 5 shows that in the 3–5 μm region lichen actually *increases* the reflectance of a sandstone as areal coverage increases, except in the lichen hydrocarbon absorption bands near 3.4 μm. Thus, the average emissivities of rocks in the 3–5 μm region may be either increased or decreased by vegetation or varnish coatings, which must be borne in mind when modeling surface emissivity.

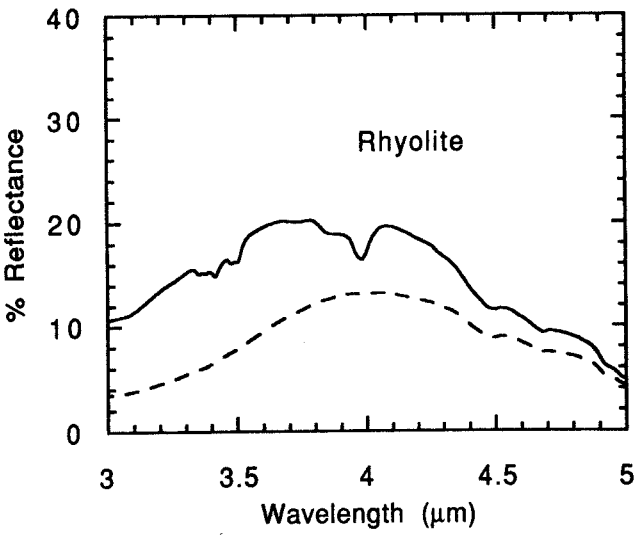

(a)

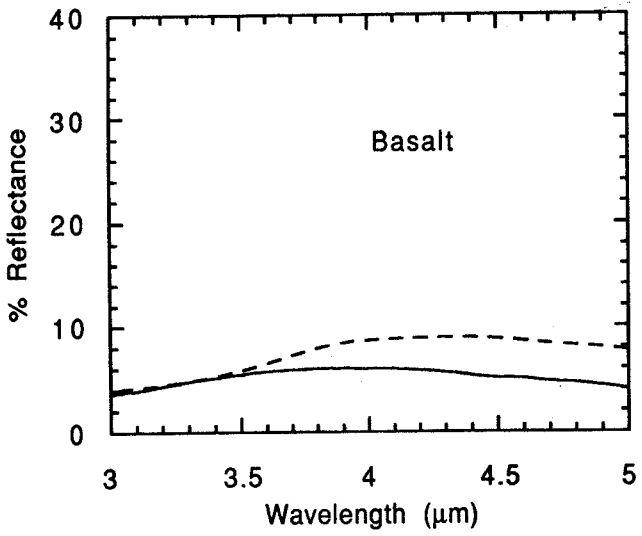

(b)

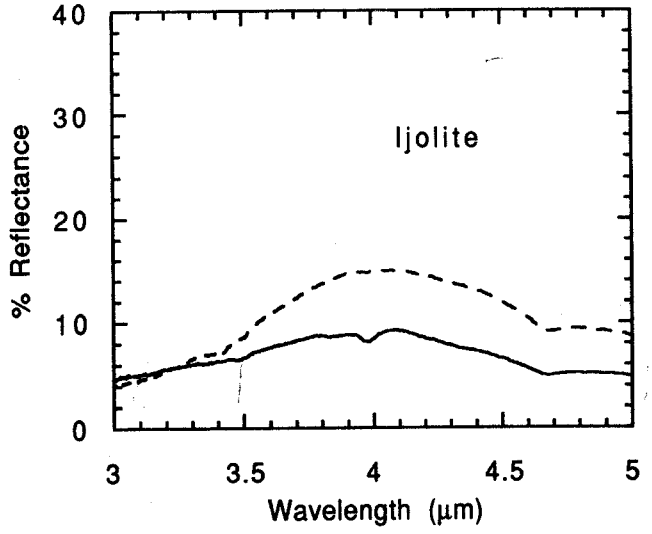

(c)

Figure 4. Directional hemispherical reflectance spectra of fresh (solid curve) and varnished (dashed curves) rock surfaces: a) rhyolite; b) basalt; c) Ijolite.

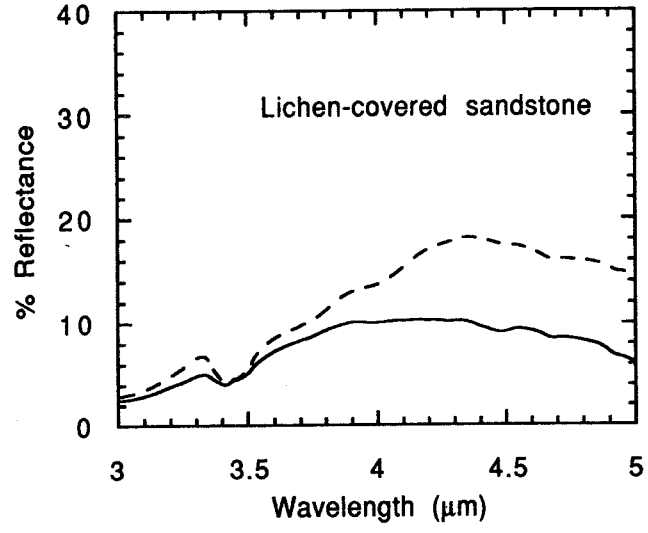

Figure 5. Directional hemispherical reflectance spectra of lichen-covered sandstone with 10% coverage (solid curve) and 65% coverage (dashed curve). Lichen was of the crustose variety.

Discussion of Rock Emissivities

The departure of reflectance from that of a black body in AVHRR Band 3 is much greater than in Bands 4 and 5 for sedimentary and metamorphic rocks. Igneous rock spectra show a large departure from black body behavior in Band 4 in addition to Band 3. For our particular collection of rocks, which we believe is fairly representative, both the magnitude of the average reflectance and the variability of reflectance in Band 3 increases from igneous (avg = 10.05, $1\sigma = 3.60$) to sedimentary (avg = 13.82, $1\sigma = 8.38$) to metamorphic rocks (avg = 18.28,

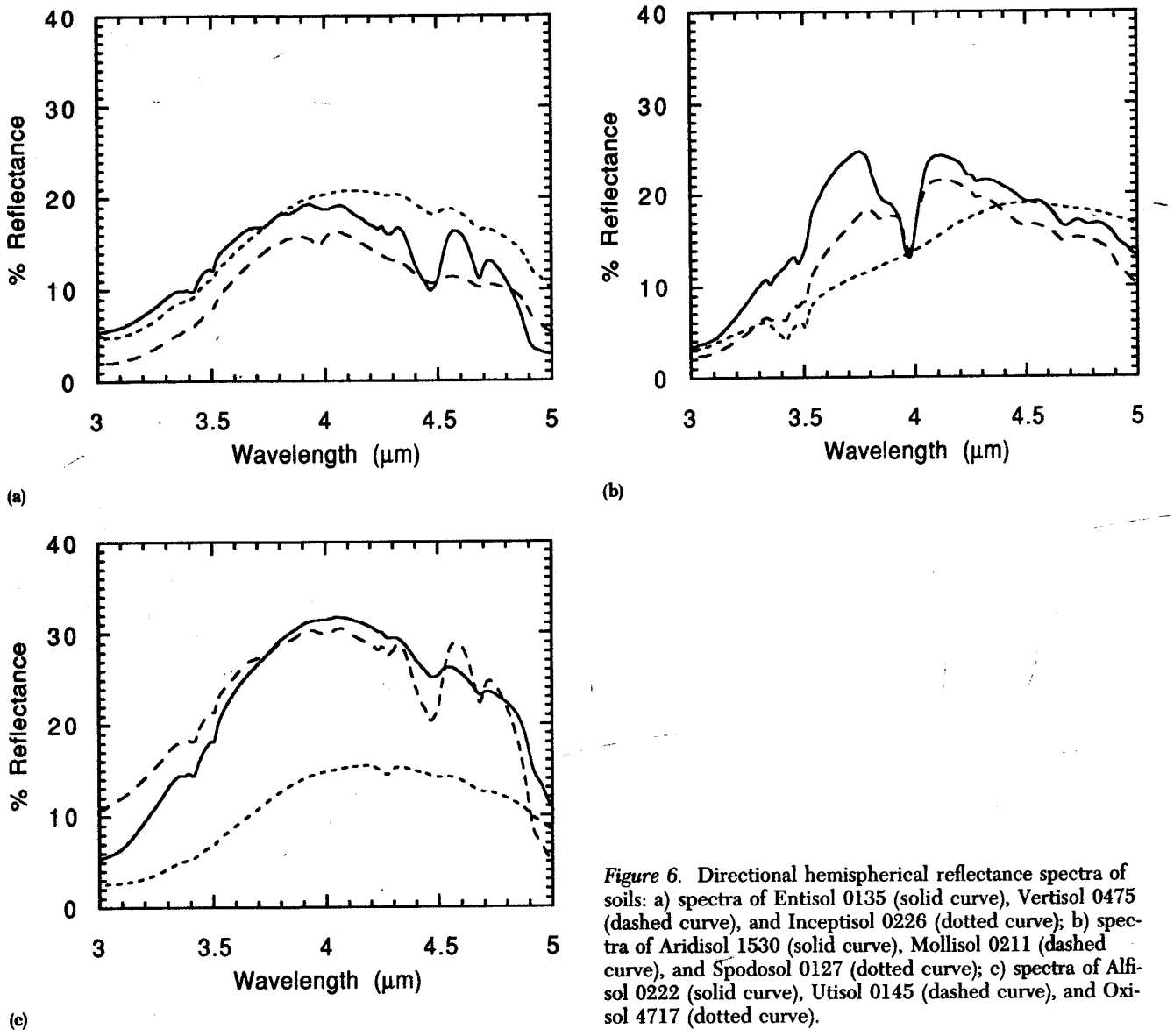

Figure 6. Directional hemispherical reflectance spectra of soils: a) spectra of Entisol 0135 (solid curve), Vertisol 0475 (dashed curve), and Inceptisol 0226 (dotted curve); b) spectra of Aridisol 1530 (solid curve), Mollisol 0211 (dashed curve), and Spodosol 0127 (dotted curve); c) spectra of Alfisol 0222 (solid curve), Utisol 0145 (dashed curve), and Oxisol 4717 (dotted curve).

$1\sigma = 11.0$). Rock coatings may alter the reflectance of rocks, but Band 3 variability and absolute reflectance typically remain greater than in Bands 4 and 5.

It is clear from the reflectance values of rocks in Table 1 that, in remote sensing of their temperature, the advantage of the lower sensitivity of Band 3 to error in estimating emissivity is more than offset by the magnitude and variability of emissivity in the Band 3 region. Band 5 provides a much more stable emissivity that is also much closer to that of a black body.

SPECTRAL BEHAVIOR OF SOILS

The complex soil classification system of the U.S. Department of Agriculture Soil Conservation Service was briefly explained in our article on the 8–14 μm spectral behavior of Earth surface materials (Salisbury and D'Aria, 1992a), and we do not repeat that explanation here. Sampling locations and brief physical descriptions of our soil samples are given in Salisbury and D'Aria (1992b). Suffice it to say here that, except for the aridisols, soil samples were obtained from all over the United States. The aridisols come primarily from the Middle East.

Soil composition is often dominated by quartz, because quartz is both a common mineral and resistant to weathering. Because of its abundance and the fact that the quartz reststrahlen bands are stronger than those of any other soil-forming minerals (Salisbury et al., 1992), quartz reststrahlen bands dominate soil spectral behavior in the 8–14 μm region. The much weaker overtone / combination tone absorption bands of quartz are seen in the 3–5 μm region, especially the strongest of these bands near 4.5 μm and 4.7 μm. These features can be

seen in Figure 6, most prominently displayed in spectra of the Entisol (Fig. 6a, solid curve) and Ultisol (Fig. 6c, dashed curve). However, weak quartz features can be seen in spectra of the Vertisol, Inceptisol, and Alfisol.

Often carbonate bands are more prominent in the 3–5 μm region than quartz bands, however, especially the strongest carbonate doublet near 4.0 μm. Such bands are best displayed in the spectra of the Aridisol (solid curve) and Mollisol (dashed curve) in Figure 6b. Soils of arid regions not only typically contain abundant carbonate, but also typically are exposed at the surface, and thus a factor in remote sensing observations. Because the carbonate bands affect emissivity in AVHRR Band 3, abundant carbonate in soil may strongly affect surface temperature estimates using this band.

Many soils are rich in organic matter, which affects their spectra. However, the organic matter in soils is not nearly as opaque as that found in shales and slates. The insoluble organic matter (kerogen) that survives weathering to be buried in shales is more carbon-rich, and hence more opaque, than soluble organic matter. Further loss of the more volatile hydrocarbons, due to high temperature metamorphism of shale to slate, results in an even more graphitic and opaque residue (Rowan et al., 1991). Thus, despite the very high (28.5%) extractable organic carbon content of the soil, the Spodosol spectrum in Figure 6b (dotted curve) has a relatively high reflectance over much of the 3–5 μm range. The Mollisol (dashed curve) has a more typical and much lower extractable organic carbon content of 2.49%, but its reflectance is not much different from that of the Spodosol. This is because the overall reflectance is controlled more by carbonate and quartz absorption bands than by the organic matter, except in the fundamental H–C stretching vibration bands at 3.4 μm and 3.5 μm.

Discussion of Soil Emissivities

The relatively fine grain size of soils, which typically contain a clay-size fraction (< 2 μm), maximizes scattering, making soil reflectances in AVHRR Band 3 greater than that for rocks (avg = 20.28 for our soil collection). Backscatter intensity is dominated by the finer particles in soils, which tend to coat the larger grains. As a result, there is relatively little variation in Band 3 reflectance ($1\sigma = 6.68$). Both Bands 4 and 5 display a much lower reflectance and variability (Band 4, avg = 3.15, $1\sigma = 0.72$; Band 5, avg = 2.43, $1\sigma = 0.45$). Thus, as in the case of rocks, Band 3 offers no advantage for remote sensing of temperature.

SPECTRAL BEHAVIOR OF VEGETATION

Lichens

As pointed out under the discussion of lichens as a rock coating material, lichens are more reflective in the 3–5 μm region than they are in the 8–14 μm. As in the longer wavelength region, however, lichens of all kinds display a remarkable uniformity of spectrum in the 3–5 μm region [compare spectrum of 65% crustose lichen cover in Fig. 5 (dashed curve) with that of the foliose variety in Fig. 7a]. As illustrated in Figure 7a, their spectra have a low reflectance in the region of the fundamental H–C stretching vibration bands near 3.4 μm and 3.5 μm, and rise to a much higher reflectance at longer wavelengths. This high reflectance occurs because they do not have the cellular water content of green leaves (see below). Different lichens in our collection vary by about 1% in reflectance at the short wavelength end of the 3–5 μm window and by about 3% at the long wavelength end.

Green Foliage

Green leaves of all kinds display a uniformly low reflectance throughout the 3–5 μm region, except for weak reststrahlen reflectance peaks near 3.43 μm and 3.51 μm associated with the H–C vibration bands, as shown in Figure 7b. These vibration bands are expressed as reflectance peaks, rather than troughs, because of the dominance of surface scattering. Volume scattering, which would cause absorption bands, is virtually eliminated due to very strong absorption by cellular water in the leaves, which absorbs any photons that penetrate the surface. Like most surface scattering reststrahlen bands, these features are offset to slightly longer wavelength than the absorption band minima resulting from volume scattering (Salisbury et al., 1992).

Senescent Foliage

The spectral reflectance of senescent leaves and pine needles varies sharply from that of green materials, primarily because of the loss of cell water, but also because the waxy cuticle flakes off of the broad leaves after senescence. As in the 8–14 μm region, the spectra of the broad leaves (solid and dashed curves) and dry rye grass (dotted curve) shown in Figure 7c are close to that of pure cellulose, while that of pine needles (dash-dot curve) is less reflective and more featureless. Without water present to absorb photons penetrating the surface of the senescent broad leaves and grass, volume scattering results in absorption band troughs in the hydrocarbon bands near 3.4 μm and 3.5 μm. However, reflectance from the pine needles does display some surface scattering, presumably because the resinous material of the needle is highly absorptive, with or without water present.

Bark

The similarity of spectra of different barks in Figure 7d reflects the fact that all bark is lignified cellulose. The differences in overall reflectance are apparently related to differences in texture, which modifies scattering.

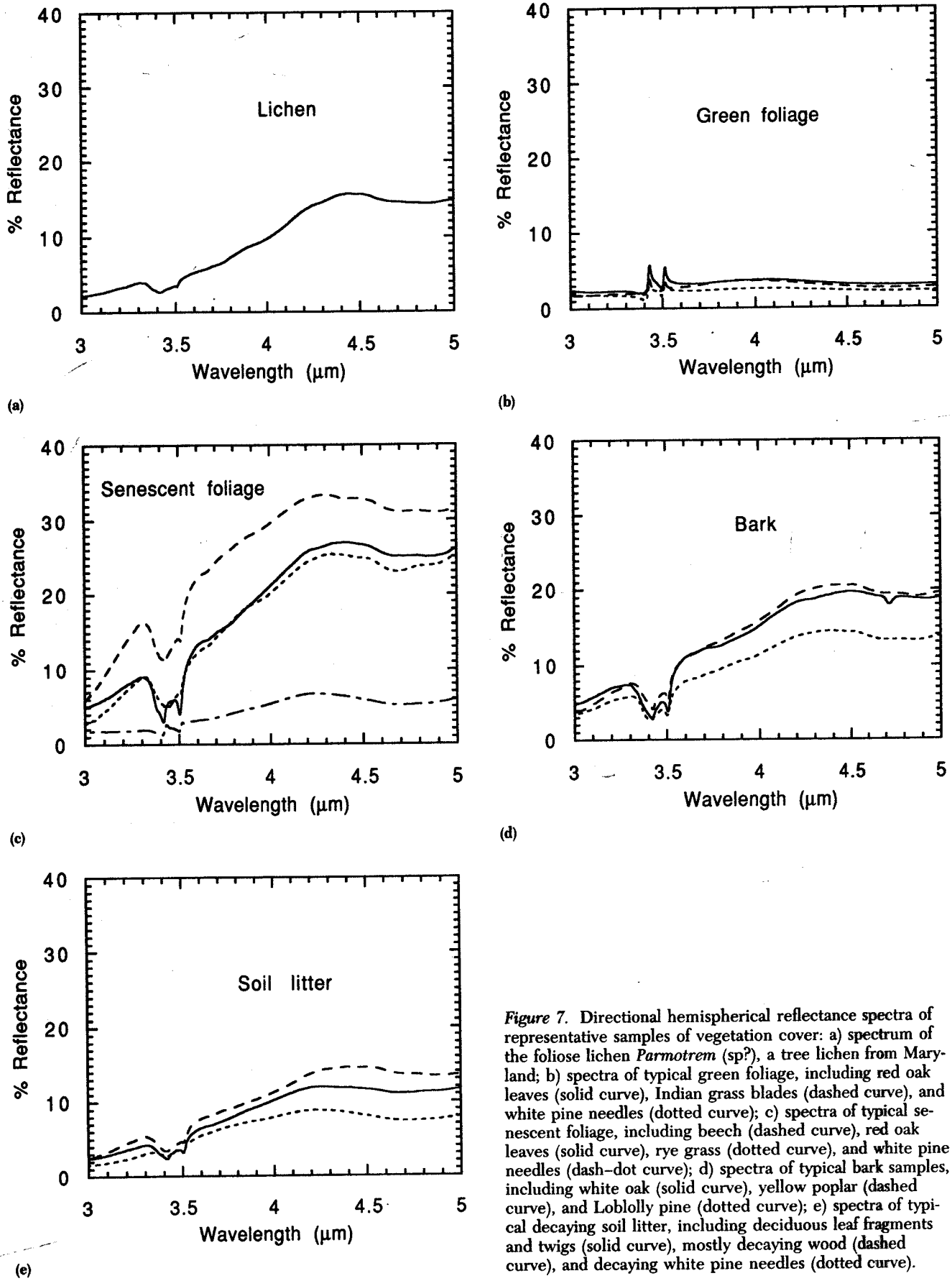

Figure 7. Directional hemispherical reflectance spectra of representative samples of vegetation cover: a) spectrum of the foliose lichen *Parmotrem* (sp?), a tree lichen from Maryland; b) spectra of typical green foliage, including red oak leaves (solid curve), Indian grass blades (dashed curve), and white pine needles (dotted curve); c) spectra of typical senescent foliage, including beech (dashed curve), red oak leaves (solid curve), rye grass (dotted curve), and white pine needles (dash–dot curve); d) spectra of typical bark samples, including white oak (solid curve), yellow poplar (dashed curve), and Loblolly pine (dotted curve); e) spectra of typical decaying soil litter, including deciduous leaf fragments and twigs (solid curve), mostly decaying wood (dashed curve), and decaying white pine needles (dotted curve).

Soil Litter

Spectra of decaying soil litter are shown in Figure 7e. Freshly fallen leaves, bare wood, and dry grass display the spectrum of cellulose but, as this material begins to decay, its spectrum becomes flatter and less reflective. In the previous article (Salisbury and D'Aria, 1992a), we suggested that the ultimate reflectance of fully decayed organic materials is probably well represented by the spectrum of the organic-rich Spodosol surface horizon shown in Figure 6b (dotted curve). While this may be true in the 8–14 μm region, the overall reflectance of the soil is higher than that of our litter samples, probably because of the presence of some fine quartz in the soil.

Discussion of Vegetation Emissivity

Lichens. Lichens may be locally abundant on the surfaces of rock types favorable for their growth, especially in high alpine and Arctic climates. However, complete coverage is rare and lichens appear slightly transparent (1–2%) to rock reflectance as well. Thus, lichens can be a locally significant factor in rock reflectance, but do not typically dominate over large areas.

Green vegetation. Green vegetation, on the other hand, can completely cover a large surface. Based on their reflectance, the emittance from individual leaves and conifer needles is close to that of a black body in the 3–5 μm region. As discussed in our previous article (Salisbury and D'Aria, 1992a), black body behavior will be enhanced by canopy scattering. Thus, closed canopies can reasonably be assigned an emissivity of 1.0. Clearly, this value must decrease as vegetation becomes sparse and soil or soil litter and bark contribute to emittance. However, emissivity should remain close to 1.0 as long as the leaf area index is great enough to suggest multiple scattering in the canopy.

AVHRR Bands 3, 4, and 5 display about the same reflectances for green vegetation. Thus, from emissivity considerations alone, the lower sensitivity of Band 3 to emissivity errors is an advantage for remote sensing of the temperature of green vegetation. The greater energy available in Bands 4 and 5, and the lesser effect of atmospheric water vapor on energy received at the sensor in these bands, are additional variables not considered here. Obviously, these considerations might dictate the use of the longer wavelength bands, despite the greater effect of emissivity error in those bands.

Senescent vegetation. Emittance from individual senescent broad leaves in the 3–5 μm region is very far from that of a black body, as is that of bark. Thus, deciduous forests in the Fall, with individual trees surrounded by fallen leaves, may display an emissivity sufficiently far from black body behavior in AVHRR Band 3 to counteract any emissivity error advantage compared to Bands 4 and 5. This is also true for dried grass, while conifers would be expected to retain an emissivity of essentially 1.0 in all bands at all seasons. Thus, there is a seasonal effect that must be considered along with cover type in assigning emissivities to forested or grassland surfaces.

SPECTRAL BEHAVIOR OF WATER

Sea Water

Water is often assumed to have an emissivity of 1.0, but it is well known that this is not true (Pinkley and

Figure 8. a) Directional hemispherical reflectance spectra of sea water (solid curve) and sea foam (dashed curve). b) Directional hemispherical reflectance spectra of distilled water with suspended quartz sediment: Solid, dashed, and dotted curves represent spectra recorded at 7, 23, and 64 min after mixing, as the quartz grains settle out; these curves overlap so closely that they cannot be distinguished.

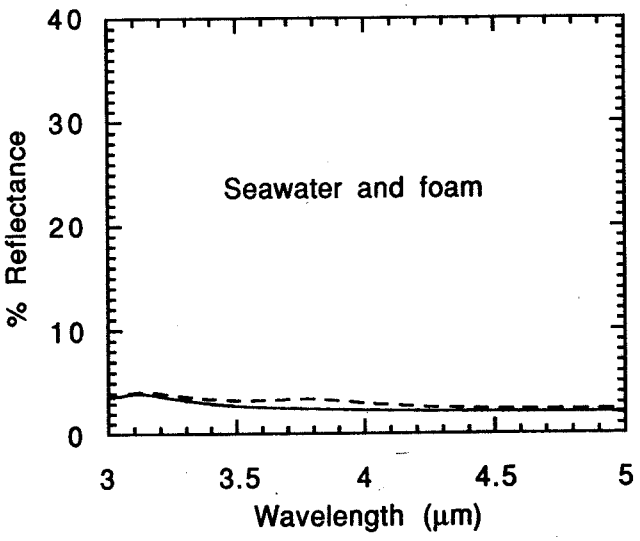

(a)

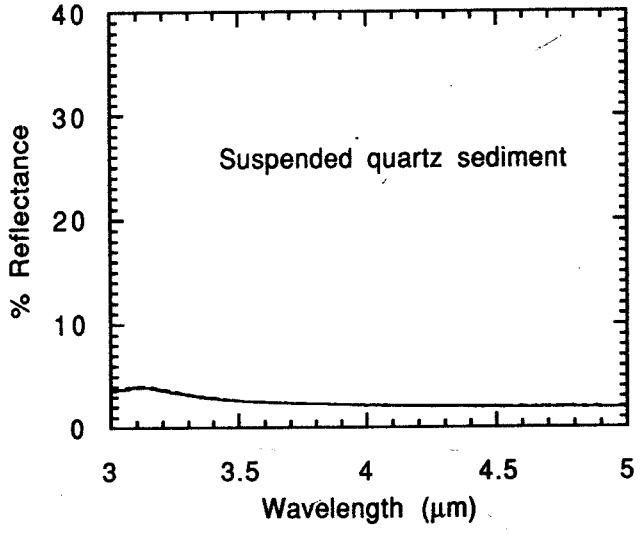

(b)

Williams, 1976), as we illustrated in our previous article (Salisbury and D'Aria, 1992a) for the 8–14 μm region. Figure 8a (solid curve) shows the directional hemispherical reflectance of sea water in the 3–5 μm region. Although Pinkley and Williams (1976) point out the small spectral differences between distilled water and sea water, these differences are too small to affect most temperature estimates. In fact, they are of the same magnitude as small differences in emissivity expected from temperature changes alone (Pinkley et al., 1977).

To this point, we have not considered the effects of the bi-directional reflectance function (BDRF) on reflectance and emissivity, because the materials considered so far have had rough surfaces or complex canopies from which we expect generally uniform directional spectral behavior, except perhaps at grazing angles (Norman et al., 1990). Water may differ in this regard, because of its exceptional range of possible surface roughness. However, Fresnel equation calculations of directional reflectance based on the optical constants of Pinkley et al. (1977) show that there is little effect until an angle of about 45° is reached (see also Fig. 3-111 in Wolfe and Zissis, 1989). At that point, reflectance begins to rise, but the shape of the spectral curve remains constant. The statistical distribution of wave slopes, which is largely a function of wind speed (Cox and Munk, 1954), can be combined with calculated directional reflectance to yield an average reflectance or emissivity under different sea surface conditions.

Despite its high absorption coefficient, water does not entirely obscure the reststrahlen bands of suspended sediment in the 8–14 μm region, at least when that sediment is quartz with very strong reflectance peaks (Salisbury and D'Aria, 1992a). However, Figure 8b shows that suspended sediment, lacking strong bands in the 3–5 μm region, has no effect on water reflectance there.

Ice

Salisbury and D'Aria (1992a) made preliminary spectral measurements of sea water ice and distilled water ice which showed that the spectra of smooth samples differed substantially in the 8–14 μm region, while roughening the surfaces with 100 grit sandpaper resulted in very strong spectral similarity. The spectral similarity of rough surfaces was attributed to the similarity of absorption coefficient of the two ices, which is the most important parameter when volume scattering dominates reflectance. Surface scattering becomes more important for smooth surfaces and involves the refractive index as well as the absorption coefficient, so it was concluded that sea water ice and distilled water ice differed in refractive index to account for their spectral differences when smooth. What was not offered was an explanation of how this can occur. Such differences in refractive index occur, despite similar absorption coefficients, because of differences in lattice vibrations. It is reasonable to assume that the presence of dissolved salt would, indeed, distort the crystal lattice, while the fundamental absorption coefficient of water ice could remain unchanged.

Whatever the cause of spectral differences in the 8–14 μm region, the two kinds of ice appear quite similar in their spectral behavior in the 3–5 μm region. The relative heights of the reflectance peak near 3.1 μm in Figure 9a may be due to small differences in surface roughness of these particular samples, as other

Figure 9. Directional hemispherical spectra of sea water ice (solid curves) and distilled water ice (dashed curves): a) original smooth surfaces; b) after roughening with 100-grit sandpaper.

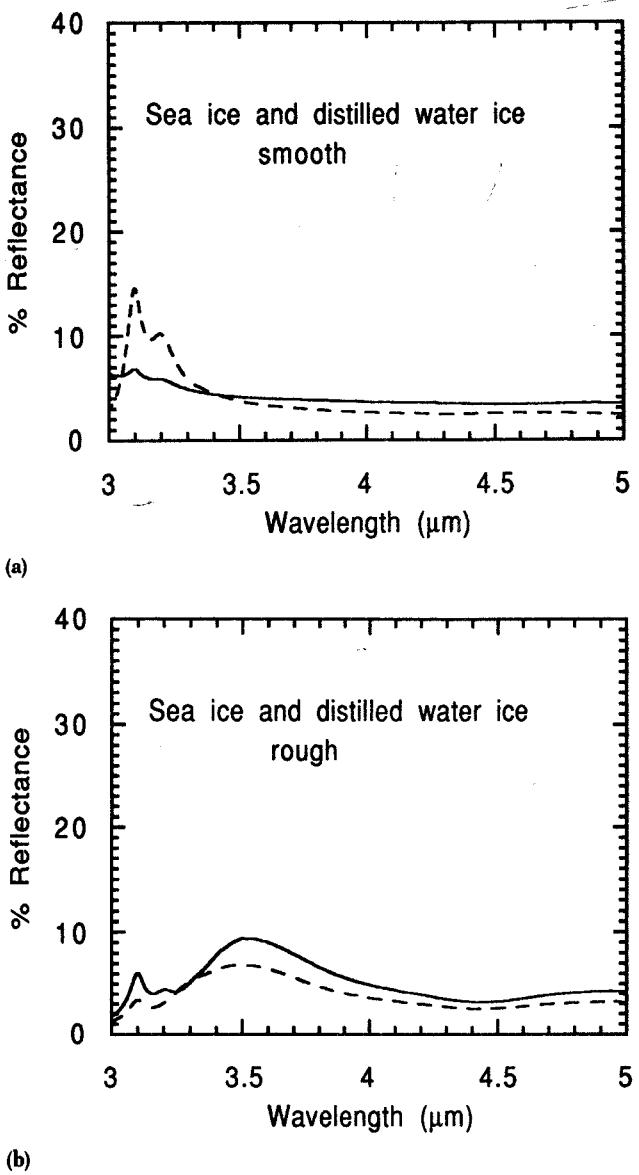

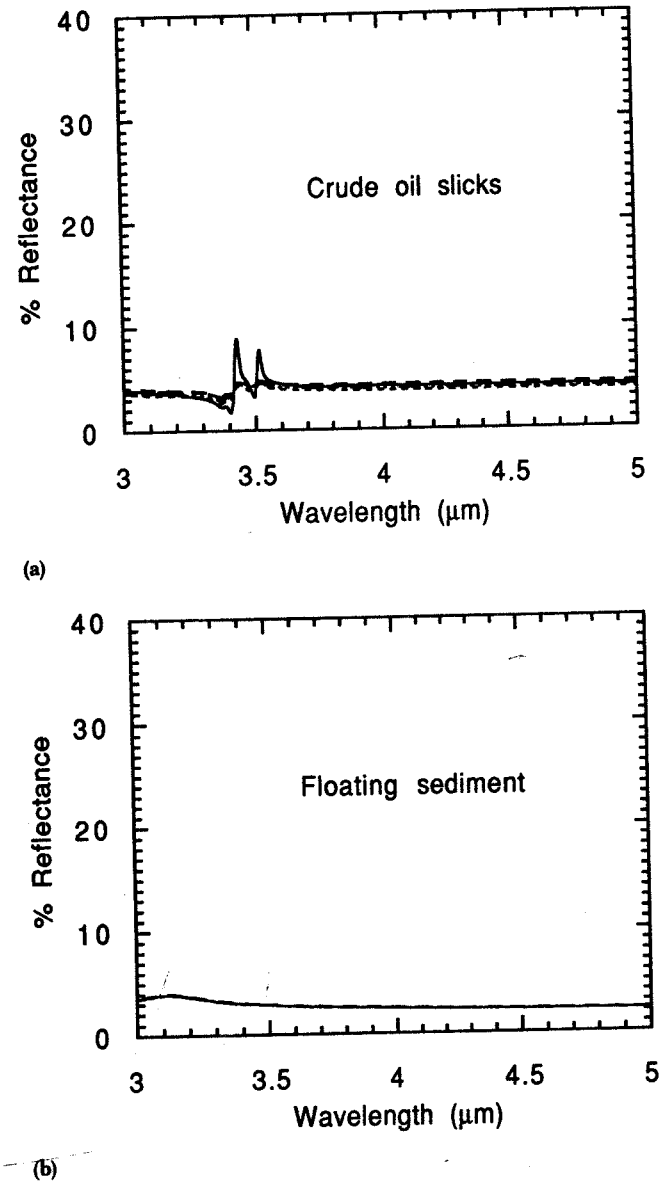

Figure 10. Directional hemispherical reflectance spectra of floating materials on water: a) continuous oil slicks 2–3 mm thick on sea water made with five different crude oil samples; b) patchy monolayers of very fine windblown quartz powder (solid curve) and a montmorillonitic soil (dashed curve) floating on tap water; these curves overlap so closely that they cannot be distinguished.

samples showed more similar spectral features here. It is, in any event, the spectral behavior of rough surfaces that are of most importance, because we expect most natural ice surfaces to be rough. The biggest spectral change from smooth to rough surfaces is the introduction of a broad reflectance maximim centered about 3.5 μm. While there appears to be a minor shift in the peak of this maximum for sea ice compared to distilled water ice and average reflectances in AVHRR Band 3 differ by about 1%, we conclude that all ice has essentially the same spectral signature when rough, which was our conclusion in the 8–14 μm region as well.

Coatings

Different coatings on water naturally may change its spectral behavior. Common coatings are foam, oil slicks, and windblown dust.

Volume scattering in bubbles makes sea foam bright in the visible, but our previous article (Salisbury and D'Aria, 1992a) showed that the absorption coefficient of water is so high in the 8–14 μm region that negligible volume scattering takes place in foam bubbles. Consequently, foam is not brighter than sea water in the 8–14 μm region. This is also true in the 3–5 μm region, as indicated by the fact that sea water and foam have very close to the same reflectance in Figure 8a.

Crude oil slicks were made in the laboratory by pipetting known volumes of oil onto a sea water sample in a Petri dish. These oils are of very different compositions and viscosities, as described in Salisbury and D'Aria (1992a), but display virtually identical infrared spectra, as shown in Figure 10a. A detailed study of these slicks is reported in Salisbury et al. (1993). Briefly, it was found that spectra of oil slicks are flat with a reflectance of about 4% throughout the spectral range from 3–14 μm, with the exception of the small reststrahlen reflectance peaks associated with the C—H bands. This spectral behavior is essentially not affected by slick thickness or age, and can be used to detect oil slicks by its contrast with the variable spectral reflectance of water in the 8–14 μm region.

Very fine windblown dust may float on a calm water surface, supported by surface tension. Such dust particles typically agglomerate into small patches a few millimeters across, and these patches may coalesce into larger patches or streamers under the influence of slow current action. Such coatings are ephemeral and easily destroyed, but have a large effect on the spectrum of water in the 8–14 μm region, because that is where the silicate reststrahlen bands lie. In the 3–5 μm region, however, the water spectrum is unaffected by such coatings, as can be seen in Figure 10b.

Discussion of Emissivities of Water and Ice

Water. Water is closer to a black body in AVHRR Band 4 than in Bands 3 and 5, but water should provide a target with a known and relatively uniform emissivity in all bands, compared to land surfaces. Surface coatings and suspended sediment change the emissivity of water very little, except for oil slicks. However, extreme surface roughness can raise reflectance substantially in all bands, making the lower sensitivity of Band 3 to emissivity errors more attractive if surface roughness is not known.

Ice. As for ice, Band 4 offers an emissivity closer to a black body and less variable than do both Bands 3 and 5.

We are grateful to Ken Watson for a very helpful critique, and to a number of people who provided samples for measurement, including Cathy Ager for lichen samples, Larry Brown for soil samples, Michael Chenevey for varnished rhyolite and basalt samples, Doug Nash for sea water, John Norman for prairie grass samples, and Floyd Sabins for oil samples. Larry Rowan collected the sample and measured the spectrum of the fresh and varnished ijolite on spectrometer equipment similar to ours at the U.S. Geological Survey (USGS) in Reston, Virginia. Vicki Comer of the USGS identified the lichen samples. This research was supported by the Solid Earth Science Branch of the U.S. National Aeronautics and Space Administration in support of the Earth Observing System (EOS).

REFERENCES

Cox, C. and Munk, W. (1954), Statistics of the sea surface derived from sun glitter, *Sears Found. J. Mar. Res.* 13:198–227.

Drummond, J. R. (1991), Measurements of pollution in the troposphere (MOPITT), in *The Use of EOS to Study Atmospheric Physics* (J. Gille and G. Visconti, Eds.), North-Holland, Amsterdam.

Estep-Barnes, P. A. (1977), Infrared spectroscopy, in *Physical Methods in Determinative Mineralogy*, 2nd ed. (J. Zussman, Ed.), Academic, New York, Chap. 2, p. 529–603.

Farmer, V. C., Ed. (1974), *The Infrared Spectra of Minerals*, Monograph No. 4, Mineralogical Society, London, 539 pp.

Farmer, V. C., and Palmieri, F. (1975), The characterization of soil minerals by infrared spectroscopy, in *Soil Components*, Vol. 2. *Inorganic Components* (J. E. Gieseking, Ed.), Springer-Verlag, New York, pp. 573–670.

Fujisada, H., and Ono, M. (1991), Overview of ASTER design concept. *Soc. Photo-Opt. Instrum. Eng.* 1490:320–342.

Hovis, W. A., and Callahan, W. R. (1966), Infrared reflectance spectra of igneous rocks, tuffs and red sandstone from 0.5 to 22 μm, *J. Opt. Soc. Am.* 56:639–643.

Hunt, G. R., and Salisbury, J. W. (1975), *Mid-Infrared Spectral Behavior of Sedimentary Rocks*, Air Force Cambridge Research Laboratories Technical Report, TR-75-0356, Bedford, MA, 49 pp.

Hunt, G. R., and Salisbury, J. W. (1976), *Mid-Infrared Spectral Behavior of Metamorphic Rocks*, Air Force Cambridge Research Laboratories Technical Report, TR-76-0003, Bedford, MA, 67 pp.

Key, J., and Haefliger, M. (1992), Arctic ice surface temperature retrieval from AVHRR thermal channels, *J. Geophys. Res.* 97:5885–5893.

Lang, H. R., Bartholomew, M. J., Grove, C. I., and Paylor, E. D. (1990), Spectral reflectance characterization (0.4 to 2.5 and 8.0 to 12.0 μm) of Phanerozoic strata, Wind River Basin and southern Bighorn Basin areas, Wyoming, *J. Sed. Pet.* 60:504–524.

Lyon, R. J. P. (1964), *Evaluation of Infrared Spectrophotometry for Compositional Analysis of Lunar and Planetary Soils. Part II: Rough and Powdered Surfaces*, NASA-CR-100, Washington, DC, 262 pp.

McClain, E. P., Pichel, W. G., and Walton, C. C. (1985), Comparative performance of AVHRR-based multichannel sea surface temperatures, *J. Geophys. Res.* 90:11,587–11,601.

Norman, J. M., Chen, J., and Goel, N. (1990), Thermal emissivity and infrared temperature dependence of plant canopy architecture and view angle, in *Proceedings of the IEEE International Geoscience and Remote Sensing Symposium*, 20–24 May, College Park, MD, Vol. 3, IEEE, New York, pp. 1747–1750.

Pinkley, L. W., and Williams, D. (1976), Optical properties of sea water in the infrared, *J. Opt. Soc. Am.* 66:554–558.

Pinkley, L. W., Sethna, P. P., and Williams, D. (1977), Optical constants of water in the infrared: Influence of temperature, *Opt. Soc. Am.* 67:494–499.

Potter, R. M., and Rossman, G. R. (1979), The manganese and iron-oxide mineralogy of desert varnish, *Chem. Geol.* 25:79–94.

Price, J. C. (1983), Estimating surface temperatures from satellite thermal infrared data—a simple formulation for the atmospheric effect, *Remote Sens. Environ.* 13:353–361.

Rowan, L. C., Salisbury, J. W., Kingston, M. J., Vergo, N. S., and Bostick, N. H. (1991), Evaluation of visible, near-infrared and thermal-infrared reflectance spectra for studying thermal alteration of Pierre shale, Wolcott, Colorado. *J. Geophys. Res.* 96:18,047–18,057.

Salisbury, J. W., and D'Aria, D. M. (1992a), Emissivity of terrestrial materials in the 8–14 μm atmospheric window, *Remote Sens. Environ.* 42:83–106.

Salisbury, J. W., and D'Aria, D. M. (1992b), Infrared (8–14 μm) remote sensing of soil particle size, *Remote Sens. Environ.* 42:157–165.

Salisbury, J. W., Walter, L. S., and D'Aria, D. (1988), *Mid-Infrared (2.5 to 13.μm) Spectra of Igneous Rocks*, USGS Open File Report 88-686, Washington, DC, 126 pp.

Salisbury, J. W., Walter, L. S., Vergo, N., and D'Aria, D. M. (1992), *Mid-Infrared (2.1 to 25 μm) Spectra of Minerals*, Johns Hopkins University Press, Baltimore, 296 pp.

Salisbury, J. W., D'Aria, D. M., and Sabins, F. F. (1993), Thermal Infrared remote sensing of crude oil slicks, *Remote Sens. Environ.*, forthcoming.

Salomonson, V. V., Barnes, W. L., Maymon, P. W., Montgomery, H. E., and Ostrow, H. (1989), MODIS: advanced facility instrument for studies of the Earth as a system, *IEEE Trans. Geosci. Remote Sens.* 27:145–153.

Wolfe, W. L., and Zissis, G. J. (1989), *The Infrared Handbook*. Environmental Research Institute of Michigan, Ann Arbor, 1710 pp.